ARTICLE | OPEN ACCESS

Indian journal of
Engineering

To Cite:
Ve QL, Do MC, Nguyen TC, Nguyen QH, Nguyen QL, Mahmoudi F. Thin film theory and boundary layer theory, an approach for analysing heat and mass transfer in spacer-filled Direct Contact Membrane Distillation. *Indian Journal of Engineering*, 2024, 21, e4ije1679
doi: https://doi.org/10.54905/disssi.v21i55.e4ije1679

Author Affiliation:
[1]Faculty of Engineering and Food Technology, University of Agriculture and Forestry, Hue University, Thua Thien Hue 530000, Vietnam
[2]School of Engineering and Technology, Hue University, Thua Thien Hue 530000, Vietnam
[3]The Commonwealth Scientific and Industrial Research Organisation (CSIRO), Private Bag 10, Clayton South, VIC, 3169, Australia

[*]**Corresponding Author**
Faculty of Engineering and Food Technology, University of Agriculture and Forestry, Hue University, Thua Thien Hue 530000, Vietnam
Email: vqlinh@hueuni.edu.vn; vequoclinh@huaf.edu.vn

Peer-Review History
Received: 05 March 2024
Reviewed & Revised: 09/March/2024 to 13/May/2024
Accepted: 16 May 2024
Published: 23 May 2024

Peer-Review Model
External peer-review was done through double-blind method.

Indian Journal of Engineering
pISSN 2319–7757; eISSN 2319–7765

DISCOVERY
SCIENTIFIC SOCIETY

Thin film theory and boundary layer theory, an approach for analysing heat and mass transfer in spacer-filled Direct Contact Membrane Distillation

Quoc Linh Ve[1*], Minh Cuong Do[1], Thanh Cuong Nguyen[1], Quoc Huy Nguyen[1], Quang Lich Nguyen[2], Farzaneh Mahmoudi[3]

ABSTRACT

Heat and mass transfer in spacer-filled direct contact membrane distillation were experimentally investigated and explained in more detail based on the combination of the thin film theory and boundary layer theory. Experimental results were used to calculate mass transfer coefficient through the boundary layer instead of existing Sherwood number correlations or modeling results. Consequently, the change of direct contact membrane distillation (DCMD) performance in terms of mass fluxes, temperature polarization coefficient (TPC), and concentration polarization coefficient (CPC) could be analyzed more clearly through the fluctuation of mass transfer coefficient through the boundary layer, and boundary layer thickness. Moreover, the results also revealed that the effect of membrane pore size on the mass transfer coefficient through the boundary layer, boundary layer thickness, and internal heat transfer coefficient was insignificant. In contrast, membrane pore size considerably influenced the membrane permeability coefficient, TPC, and CPC.

Keywords: Direct contact membrane distillation, thin film theory, boundary layer theory, heat transfer, mass transfer

1. INTRODUCTION

Membrane distillation (MD) has been becoming more popular in saline water treatment technology due to the technological breakthrough of membrane production and the implementation of renewable energy (Khayet, 2013; Khayet and Matsuura, 2011). Direct contact membrane distillation (DCMD) has been more attractive than other technologies due to its simple configuration (Khayet

and Matsuura, 2011; Ashoor et al., 2016). The temperature difference at the membrane surface causes the transmembrane vapour pressure gradient allowing the water molecules to transport to permeate side from feed side through membrane pores in DCMD (Khayet and Matsuura, 2011; Drioli et al., 2015). Although all DCMD experiments are conducted under identical conditions, the variance in permeate production in DCMD can be attributed to two factors. The initial factor is the varying design and configurations of the DCMD module and the membrane morphology, which results in inaccuracies in mass transfer calculations (Khayet and Matsuura, 2011; Schofield et al., 1990).

In addition, thermal and concentration boundary layers were another factor considered in DCMD modeling (Lokare and Vidic, 2019; Bouchrit et al., 2015; Andrjesdóttir et al., 2013; Khayet, 2011; Martínez-Díez et al., 2000; Sudoh et al., 1997). Most previous studies applied the existing heat transfer correlations to determine the Nusselt number (Nu) in DCMD with or without turbulent promoter. Then, the internal heat transfer coefficient is defined (Tewodros et al., 2022). If the saline solution was on the feed side of DCMD, mass transfer phenomena should consider the concentration polarization effect. The mass flux tends to decrease owing to this effect (Khayet, 2011; Plamenov, 2017; El-Bourawi et al., 2006; Qtaishat et al., 2008; Chen et al., 2009). To enhance the accuracy of concentration polarization coefficient (CPC) estimation, it is essential to theoretically determine the solution concentration at the feed membrane surface (Bouchrit et al., 2015; Andrjesdóttir et al., 2013; Khayet, 2011; El-Bourawi et al., 2006).

Experimental methods cannot define this parameter (Khayet, 2011; El-Bourawi et al., 2006; Camacho et al., 2013). To solve this problem, the analogy between heat and mass transfer (in Table 1) Lokare and Vidic, (2019), Qtaishat et al., (2008), Schofield et al., (1990), Bahmanyar et al., (2012), Ve et al., (2021a), or the simulated results Chang et al., (2017), Katsandri, (2017a), Katsandri, (2017b), Saeed et al., (2015), Taamneh and Bataineh, (2017) are applied to define Sherwood number. Then, the mass transfer coefficient of particles through the boundary layer is defined. However, these methodologies had their constraints. The mass transfer characteristics don't appear to be sufficiently explained under various operating conditions due to the reliance on the Sherwood number or simulated work for the mass transfer coefficient. As a result, it is necessary to explore another method that is independent of the Sherwood number correlation to determine the mass transfer coefficient through the boundary layer.

Table 1 Mass transfer correlation applied in DCMD with or without turbulent promoter;

Mass transfer correlation	Flow condition	Ref.
$Sh=1.86\left(Re\times Sc\times\frac{D_h}{L}\right)^{0.33}$	Laminar	(Alkhudhiri et al., 2012; Banat and Simandl, 1998; Khalifa et al., 2017; Martínez and Florido-Díaz, 2001; Martínez-Díez and Vázquez-González, 1999; Yun et al., 2006)
$Sh = 1.62\left(Re\times Sc\times\frac{D_h}{L}\right)^{1/3}$	Laminar	(Alkhudhiri et al., 2012)
$Sh = 0.023\,Re^{0.8}\times Sc^{1/3}$	Turbulent	(Bouchrit et al., 2015; Schofield et al., 1990; Bahmanyar et al., 2012; Alkhudhiri et al., 2012; Banat and Simandl, 1998; Khalifa et al., 2017; Yun et al., 2006; Olatunji and Camacho, 2018)
$Sh = 0.13\,Re^{0.64}\times Sc^{0.38}$	Laminar	(Bouchrit et al., 2015; Bahmanyar et al., 2012; Olatunji and Camacho, 2018)
$Sh = 0.664\times k_{dc}\times Re^{0.5}\times Sc^{0.33}\times\left(\frac{2d_h}{l_m}\right)^{0.5}$	Laminar	(Yun et al., 2011)
$Sh = 0.664\times Re^{0.5}\times Sc^{0.33}\times\left(\frac{d_h}{l_m}\right)^{0.5}$	Laminar	(Saeed et al., 2015; Shakaib et al., 2009)
$Sh = 0.023\times\emptyset_\mu\times Re^{0.8}\times Sc^{1/3}$ ϕμ Sieder-Tate heating/cooling correction	Turbulent	(Andrjesdóttir et al., 2013; Lawson and Lloyd, 1997)
$Sh = 1.47\times\left(Re\times Sc\times\frac{t}{L}\right)^{1/4}$	Laminar	(Li et al., 2002)
$Sh = 0.065\times Re^{0.875}\times Sc^{0.25}$	Laminar	(Schock and Miquel, 1987)

$Sh = 0.023 \times Re^{0.875} \times Sc^{0.25}$	Turbulent	(Alkhudhiri et al., 2012)
$Sh = 2 \times Re^{0.483} \times Sc^{1/3}$	Laminar	(Alkhudhiri et al., 2012)
$Sh = 0.0588.Re^{0.55}.Sc^{0.33}$	Laminar	(Ve et al., 2021a)

Ve et al., (2021a) has proposed an approach that combined thin film theory and boundary layer theory to find out the mass transfer correlation through boundary layer in spacer-filled DCMD. The study investigated the impact of feed inlet temperature, velocity, and feed concentration on mass transfer with various spacers. The relationship between operating conditions and boundary layer thickness, mass transfer coefficient, and shear stress are clearly explained based on this approach. However, this research didn't reveal the impact of the operating conditions on the fluctuation in permeate flux, temperature polarization coefficient (TPC), and CPC.

Furthermore, this research didn't investigate the effect of different commercial membranes on the change in DCMD performance. This study aims to clarify the fluctuation mass fluxes, TPC, and CPC through the implication of thin film theory and boundary layer theory under the impact of different operating conditions, as shown in (Figure 1). Furthermore, the effect of membrane pore size on the DCMD performance was explained more clearly based on this approach regarding the analysis of the mass transfer coefficient of particles, mass transfer coefficient through membrane pore, and boundary layer thickness.

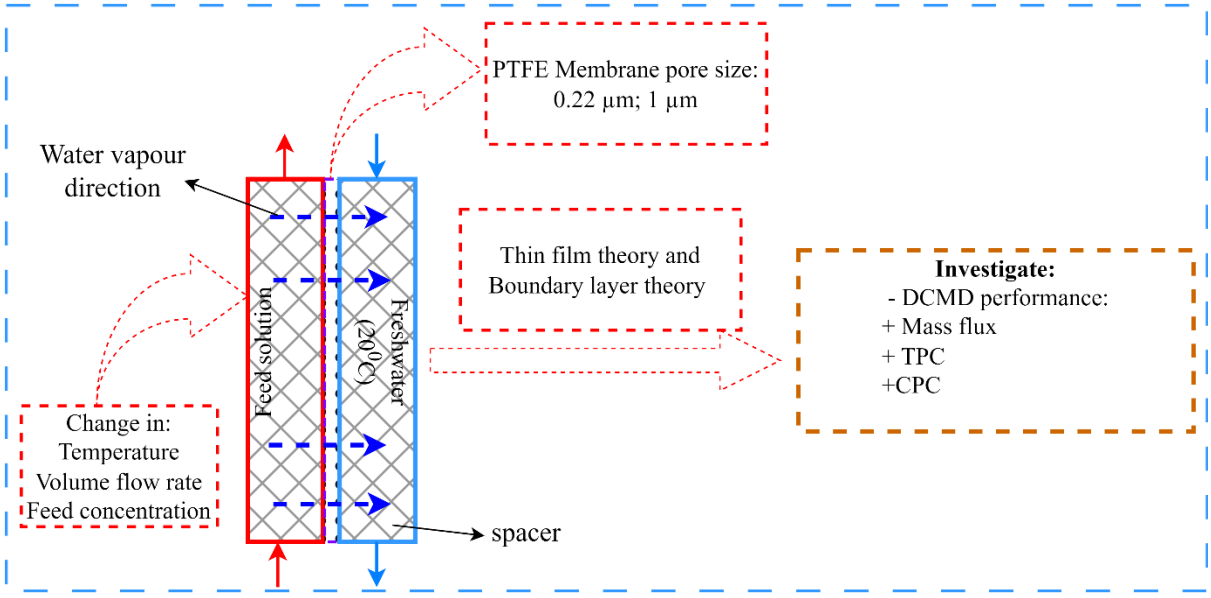

Figure 1 The entire framework of this study

2. THEORY

Heat transfer

Direct contact membrane distillation is a complex process involving both heat and mass transfer. Initially, the convective heat is transferred across the liquid boundary layer to the membrane surface at the feed side. Then, heat in the form of conduction and vapour latent heat passes through membrane pores. Finally, the convective heat is removed from the membrane surface across the liquid boundary layer on the permeate side.

The heat transfer rate across the boundary layer of both sides of the DCMD module:

$$Q_f = h_f \times A \times (T_f - T_{m,f}) \quad (1)$$

$$Q_p = h_p \times A \times (T_{m,p} - T_p) \quad (2)$$

The heat transfer rate through the membrane can be expressed (Khayet and Matsuura, 2011):

$$Q_m = \frac{k_m}{\delta_m} \times A \times (T_{m,f} - T_{m,p}) + J_w \times A \times \Delta H_{v,w} \quad (3)$$

The thermal conductivity of membrane (k_m) is calculated according to the Maxwell (Type II) model, as mentioned in previous studies (García-Payo and Izquierdo-Gil, 2004; Ve et al., 2021b)

$$k_m = \frac{k_g[1 + 2\beta\varphi + (2\beta^3 - 0.1\beta)\varphi^2 + 0.05\varphi^3\, exp(4.5\beta)]}{1 - \beta\varphi} \quad (4)$$

$$\beta = (k_p - k_g)/(k_p + 2k_g);\ \varphi = 1 - \varepsilon_m$$

At the steady state:

$$Q_f = Q_m = Q_p \quad (5)$$

The feed and permeate membrane surface temperature can be calculated from Equations (1), (2), (3), (5):

$$T_{m,f} = \frac{h_m\left(T_p + \frac{h_f}{h_p}T_f\right) + h_f T_f - J_w \Delta H_{v,w}}{h_m + h_f\left(1 + \frac{h_m}{h_p}\right)} \quad (6)$$

$$T_{m,p} = \frac{h_m\left(T_f + \frac{h_p}{h_f}T_p\right) + h_p T_p + J_w \Delta H_{v,w}}{h_m + h_p\left(1 + \frac{h_m}{h_f}\right)} \quad (7)$$

The heat transfer coefficients hi, and the overall heat transfer coefficient (H) are determined by Eq. (8) and Eq. (9):

$$h_i = \frac{Nu_i \times k_i}{d_h} \quad (8)$$

$$H = \left[\frac{1}{h_f} + \frac{1}{k_m/\delta_m + J_w \Delta H_{v,w}/(T_{m,f} - T_{m,p})} + \frac{1}{h_p}\right]^{-1} \quad (9)$$

In this investigation, the spacer altered the flow direction; therefore, the Nusselt number in the feed and permeate side (Nui) can be evaluated:

$$Nu_i = 0.664 k_{dc}\, Re_i^{0.5}\, Pr_i^{0.33}\left(\frac{2d_h}{l_m}\right)^{0.5}$$

$$k_{dc} = 1.654\left(\frac{d_f}{t_s}\right)^{-0.039} \varepsilon^{0.75}\left(\sin\left(\frac{\theta}{2}\right)\right)^{0.086} \quad (10)$$

The spacer characteristics are showed in (Table 2). Based on those measurements, the hydraulic diameter (dh), and spacer porosity (ε) were calculated (Ve et al., 2019).

Table 2 Spacer characteristics used in the DCMD module

Spacer characteristics	Measured values
Filament diameter, (df)	0.0009 (m)
Mesh length, (lm)	0.0036 (m)
Spacer thickness, (ts)	0.0016 (m)
Hydrodynamic angle, (θ)	130 ^{0}
Voidage, (ε)	0.7116

Mass transfer in DCMD

Within the DCMD process, mass transfer comprises two steps: the volatile component moves across the boundary layers to the feed-membrane surface and traverses the membrane pores. Assuming that measured mass flux is proportional to the difference between vapor pressures at both sides, the mass transfer through the membrane itself can be expressed (Qtaishat et al., 2008; Ve et al., 2021a; Lawson and Lloyd, 1997; Schofield et al., 1987; Khayet et al., 2001):

$$J_w = C_m\left(p_{v,sf} - p_{v,sp}\right) \quad (11)$$

Where the partial pressures of water vapour being a function of surface temperatures and solution salinity as explained by Antoine and Sharqawy's equations (Khayet and Matsuura, 2011; Schofield et al., 1987; Nayar et al., 2016). The membrane permeability coefficient

(Cm) was determined by (Ding et al., 2003; Ve et al., 2024). All mentioned parameters in Eq. (12) are explained in the Nomenclature section.

$$C_m=\frac{1}{RT_m\delta_m}\left[\left(\frac{3\tau}{2\varepsilon_m r}\left(\frac{\pi M}{8RT_m}\right)^{1/2}+\frac{P_a\tau}{\varepsilon_m PD}\right)^{-1}+0.125\frac{\varepsilon_m r^2 MP_m}{\tau\mu}\right] \quad (12)$$

For saline water on the feed side, predicting mass flux requires consideration of the concentration polarization effect, a crucial factor adversely affecting permeate flux. In practical scenarios, the solution concentration at the membrane surface is higher than that at bulk (Aas et al., 2017). To examine the impact of the concentration polarization effect on mass flux, thin film theory can be employed Curcio and Drioli, (2005) Eq. (13) and Eq. (14) describe the dependence of permeate flux (Jw) on the bulk solute concentration (Sf), solute concentration on the membrane surface (Sm, f), the mass transfer coefficient through the boundary layer (ks), and feed density (ϱf).

$$J_w = \rho_f k_s \, ln\left(\frac{S_{m,f}}{S_f}\right) \quad (13)$$

And

$$CPC = \frac{S_{m,f}}{S_f} = exp\left(\frac{J_w}{\rho_f k_s}\right) \quad (14)$$

ks (m.s–1) can be defined by Eq.(15):

$$k_s = \frac{D}{\delta} \quad (15)$$

Where (δ) (m) is the boundary layer thickness, and D (m2.s–1) is the diffusion coefficient of the solute, which is determined by (Boudinar et al., 1992).

$$D = \left(0.72598 + 0.023087 \times T_{m,f} + 0.00027657 \times T_{m,f}^2\right) \times 10^{-9} \quad (16)$$

Following boundary layer theory (Schlichting and Kestin, 1979), the boundary layer thickness is defined in Eq. (17).

$$\delta=\frac{5\times d_h}{\sqrt{Re_f}} \quad (17)$$

Temperature polarization

TPC is considered a limiting factor for DCMD efficiency, and TPC can be expressed using Eq. (18). The decrease of the membrane surface temperature on the feed side and the increase of the membrane surface temperature on the permeate side results in reduced partial vapor pressure difference. As a result, the reduction in the driving force resulted in a negative influence on freshwater production in the DCMD system.

$$TPC = \frac{T_{m,f} - T_{m,p}}{T_f - T_p} \quad (18)$$

Based on the TPC value, the DCMD system can be considered to have a poor or good design. If the TPC value is lower than 0.2, the DCMD process is controlled by heat transfer resistance, and this leads to a poorly designed DCMD module. If the TPC value is larger than 0.6, the DCMD process is controlled by mass transfer resistance within the membrane, and the DCMD system has a good fluid dynamic property. Usually, TPC values from 0.4 to 0.8 satisfy the DCMD module (Khayet and Matsuura, 2011; Lawson and Lloyd, 1997).

Experimental setup

In this investigation, a DCMD setup with an effective membrane of 150 x 150 mm in length, and width was established. The channel height of DCMD was 4 mm. To support the membrane, plastic spacers shown in Table 2 were placed on both sides of DCMD. Two commercial PTFE membranes with nominal pore size of 0.22 μm (PTFE022), and 1 μm (PTFE1) were applied. Both membranes had polypropylene layer support and a 75% void fraction. A solution of NaCl with 20000 ppm and 40000 ppm concentration was prepared. To measure the solution concentration in the feed and permeate side, a C-100 device was used.

On the feed side, hot saline water was heated to the appropriate temperature by BE-25L-T of 2500 W and pumped into the feed channel. On the permeate side, the CW-5000 chiller was used to cool down fresh water to a fixed temperature, which was pumped counter-currently. Four PT100 (± 0.50C) were used to measure the temperatures at inlets and outlets of feed and permeate channels. Two flowmeter sensors (±10% of the reading) were used to measure the volume flow on both sides. All the data was collected by a data

logger (DI-2108). Four pressure gauges were used to measure the pressure. Figure 2 illustrates the whole experimental setup. The operating conditions are shown in (Table 3). In each case, the experiments were repeated three times to ensure the accuracy of the measured results.

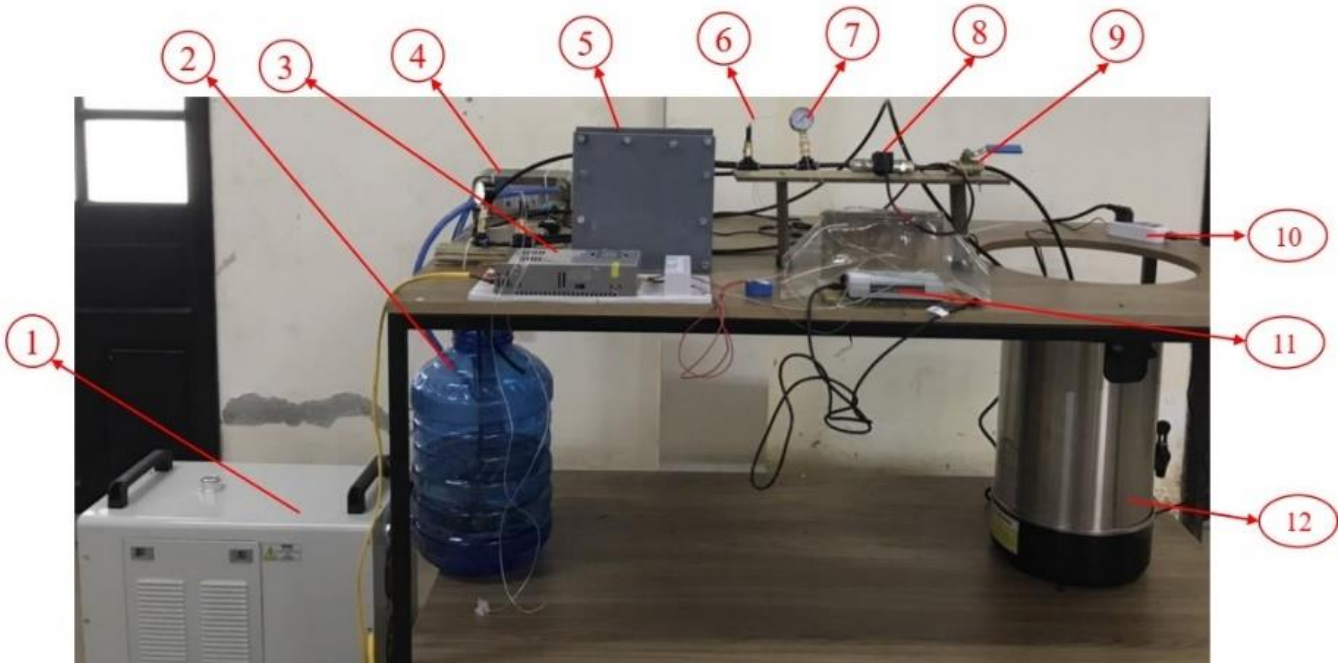

Figure 2 Experimental set-up: 1 – CW-5000 chiller; 2 – Permeate tank; 3 – Switching power supplies; 4 - Heat exchanger; 5 – DCMD module; 6 – PT100; 7 – Pressure gauge; 8 – Flowmeter sensor; 9 – Flow regulation valve; 10 – Temperature controller; 11 – Data taker; 12 – Hot solution tank.

Table 3 Experimental conditions for investigating heat and mass transfer in DCMD using PTFE022 and PTFE1

Case	Tfi (0C)	Tpi (0C)	Vf = Vp (L/s)	Sf (ppm)
I	40	20	0.03	20000
	45			
	50			
II	50	20	0.017	20000
			0.03	
III	50	20	0.03	20000
				40000

3. RESULTS AND DISCUSSIONS

Effect of feed inlet temperature on heat and mass transfer

This section examines the impact of inlet temperature at the feed side on heat and mass transfer rates. The operating conditions are the Case I of (Table 3). As can be seen from Figure 3, the experimental mass flux increased exponentially due to the increase in feed inlet temperature. The exponential relationship between partial vapor pressure and temperature was the main reason (Khayet and Matsuura, 2011; Schofield et al., 1987). Mass fluxes at 400C were 8.3 kg/m2-h, and 9.5 kg/m2-h for PTFE022 and PTFE1, respectively. At 500C, there was a significant rise of more than 93% in mass fluxes for both membranes. To conclude, the feed inlet temperature affected significantly the mass flux enhancement in DCMD (Bouchrit et al., 2015; Alkhudhiri et al., 2012; Alklaibi and Lior, 2006; Singh and Sirkar, 2014).

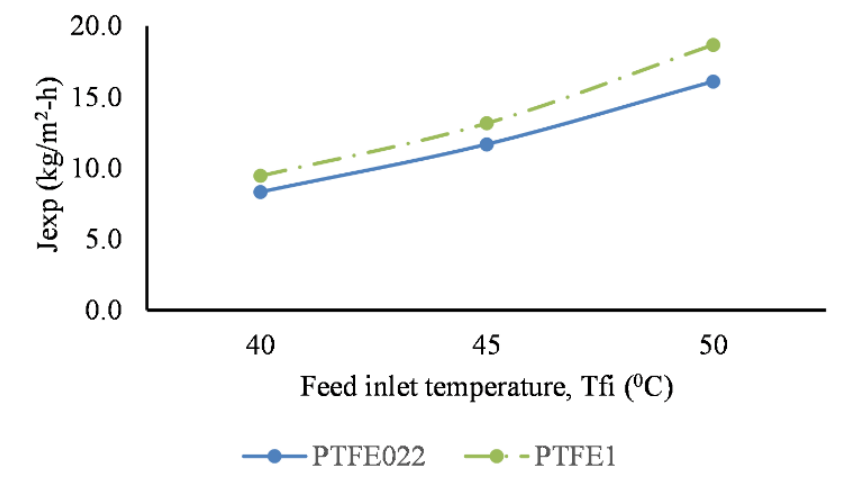

Figure 3 Experimental mass fluxes for experimental conditions in Case I

In addition, Figure 4 and Figure 5 showed that the improvement of permeate flux was also proved through the evaluation of the internal heat transfer coefficient on the feed side, the total heat transfer coefficient, the thickness of the boundary layer, and the mass transfer coefficient through the boundary layer. The rise of inlet temperature at the feed side led to the increase of both the heat transfer coefficient, and this caused the decrease in thermal boundary layer thickness (Bouchrit et al., 2015). While the hf went up unremarkably at nearly 4% for both membranes, there was a remarkable increase in the total heat transfer coefficient because of the rise in the heat of vaporization (Eq. (9)) Suleman et al., (2021), with nearly 18.5% and 19.8% for PTFE022 and PTFE1, respectively in the investigated feed inlet temperature.

There is no doubt that the boundary layer thickness dropped by nearly 8% when the inlet temperature at the feed side rose from 400C to 500C for both membranes, as shown in (Figure 5). As a result, ks increased by nearly 7.2% for the PTFE022 and PTFE1 membranes. Figure 4, and Figure 5 revealed that the pore size of the membrane didn't affect the internal heat transfer coefficient, the boundary layer thickness, as well as the mass transfer coefficient through the boundary layer. However, the pore size of the membrane influenced the membrane permeability coefficient, and the total heat transfer coefficient significantly. At 500C of feed inlet temperature, the membrane permeability coefficient and the total heat transfer coefficient for PTFE1 were more significant than that for PTFE022, with nearly 20% and 10.1%, respectively.

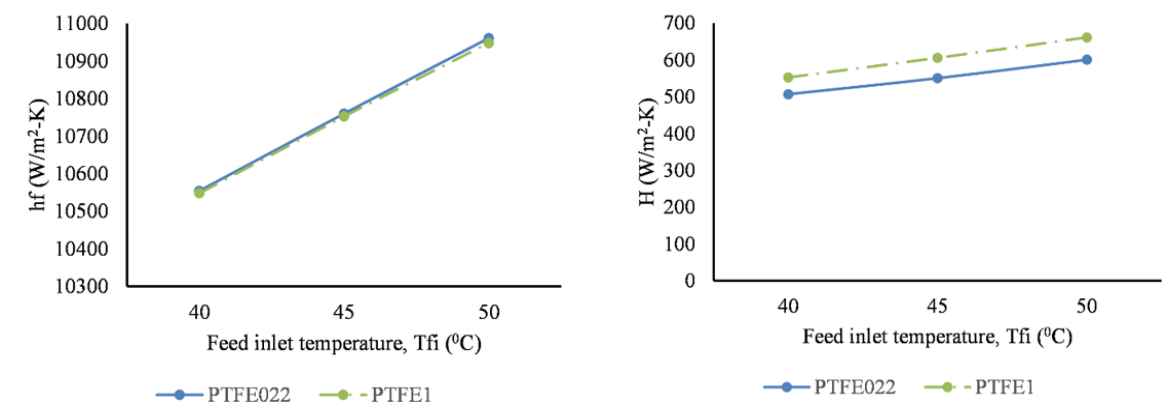

Figure 4 The impact of feed inlet temperature on (a) convective heat transfer coefficient, and (b) total heat transfer coefficient in spacer-filled DCMD channels

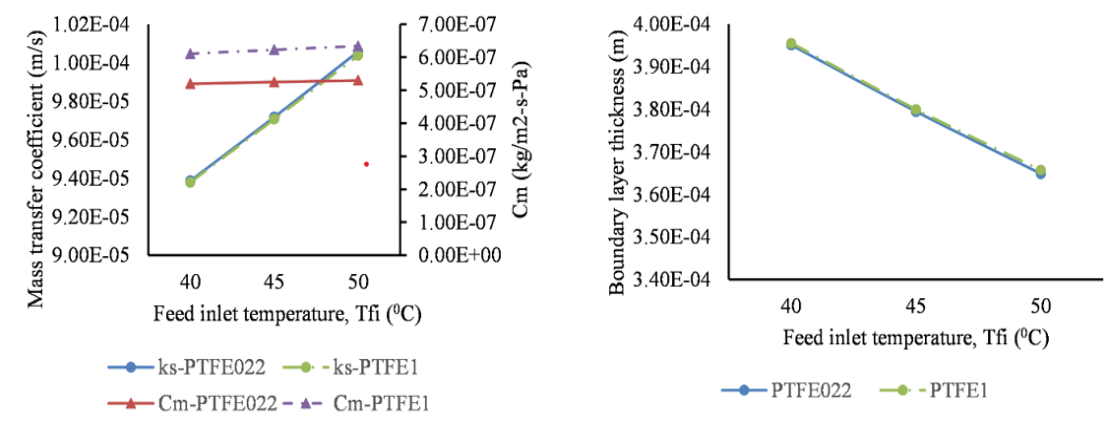

(a) (b)

Figure 5 The impact of feed inlet temperature on (a) mass transfer coefficient, and (b) boundary layer thickness in spacer-filled DCMD channels.

The fluctuation of the TPC with the feed inlet temperature was illustrated in Figure 6 when two commercial membranes with different pore sizes were implemented. In both cases of membranes, the TPC decreased insignificantly with the increase of the feed inlet temperature from 400C to 500 C (Suleman et al., 2021; Phattaranawik et al., 2003; Dittscher et al., 1994; Rodríguez-Maroto and Martínez, 2005). The improvement of permeate flux caused the drop of the TPC as the feed inlet temperature went up. In this case, the considerable temperature polarization effect was detected as the inlet temperature at the feed side rose due to the more considerable temperature discrepancy between bulk feed temperature and feed membrane surface temperature.

The PTFE022 membrane exhibited higher TPC values in contrast to the PTFE1 membrane. This discrepancy may be attributed to the smaller pore size, resulting in reduced heat transfer through vaporization. Therefore, at the feed membrane interface, the temperature drop tended to be lessened. Therefore, the temperature polarization effect (higher TPC) was less severe, and the lower mass fluxes were obtained for membranes with smaller pore size (Adnan et al., 2012).

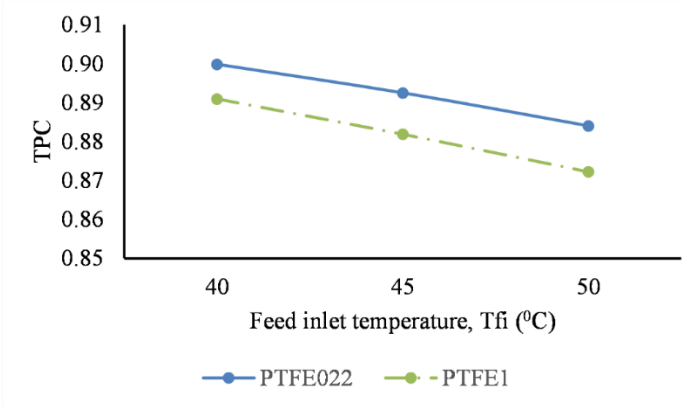

Figure 6 TPC vs. feed inlet temperature in spacer-filled DCMD configuration

From Figure 7, the CPC rose insignificantly with nearly 4.4%, and 5.5% for PTFE022 and PTFE1, respectively, when the inlet temperature at the feed side went up from 400C to 500C. The improvement of mass fluxes due to the temperature caused the rise of CPC, as shown in Eq. (14). Additionally, both shear stress and viscosity of the feed solution reduced as the feed inlet temperature rose could result in a higher fouling potential on the feed membrane interface, hence the non-volatile substance accumulated more and more. As a result, the CPC was higher as the feed inlet temperature rose (Bouchrit et al., 2015). As can be seen from Figure 7, the PTFE1 membrane had larger CPC values than that for the PTFE022 membrane. This result is due to not only the higher mass flux for PTFE1

but also the higher rate of evaporation of water molecules through the larger pore size of PTFE1. Consequently, the accumulation of non-volatile substances on the feed PTFE1 membrane surface was more than that on the feed PTFE022 membrane surface.

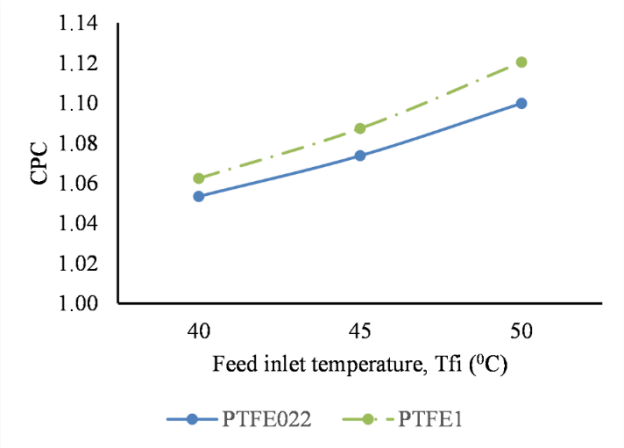

Figure 7 CPC vs. feed inlet temperature in spacer-filled DCMD configuration

Effect of volume flow rate on heat and mass transfer

The experimental conditions were the Case II of (Table 3). Through the fluctuation of the heat transfer coefficient, mass transfer coefficient through the boundary layer, and boundary layer thickness, the impact of volume flow rate and the membrane pore size on freshwater production could be explained. From Figure 8, the enhanced permeate fluxes were insignificant for both membranes. The rise in volume flow rate led to the increase of the Reynolds number, then the heat transfer coefficient rose, as shown in Eq. (8) and Eq. (10) (Ve et al., 2021a; Alkhudhiri et al., 2012).

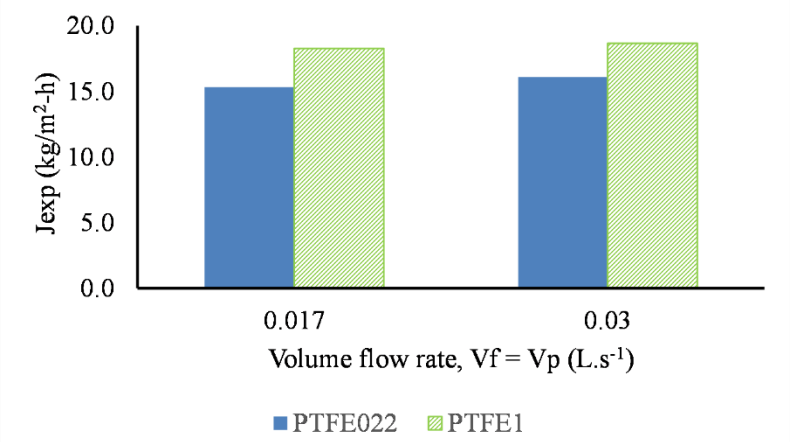

Figure 8 The influence of volume flow rate on mass flux

The heat transfer coefficient increased by approximately 33.2% at 0.03 L.s–1 compared to 0.017 L.s–1 in both membranes, as shown in (Figure 9). However, the rise of the total heat transfer coefficient was trivial because the heat of vaporization was only a function of the temperature. Also, the increase of volume flow rate caused the drop in boundary layer thickness, and then the mass transfer coefficient through the boundary layer rose, as shown in Figure 9, and Figure 10 (Alkhudhiri et al., 2012). Consequently, the mass flux increased insignificantly when the volume flow rate went up. Furthermore, the PTFE1 membrane had higher mass fluxes in comparison to the PTFE022 membrane.

The dominant factor for this result is the permeability coefficient. From Figure 10, there was an insignificant difference between the boundary layer thickness and the mass transfer coefficient through the boundary layer. However, there was a considerable difference

in permeability coefficient for PTFE022 and PTFE1 membranes. The mass transfer coefficient through the PTFE1 membrane pore was much larger, nearly 20% than that for the PTFE022 membrane in all investigated volume flow rates.

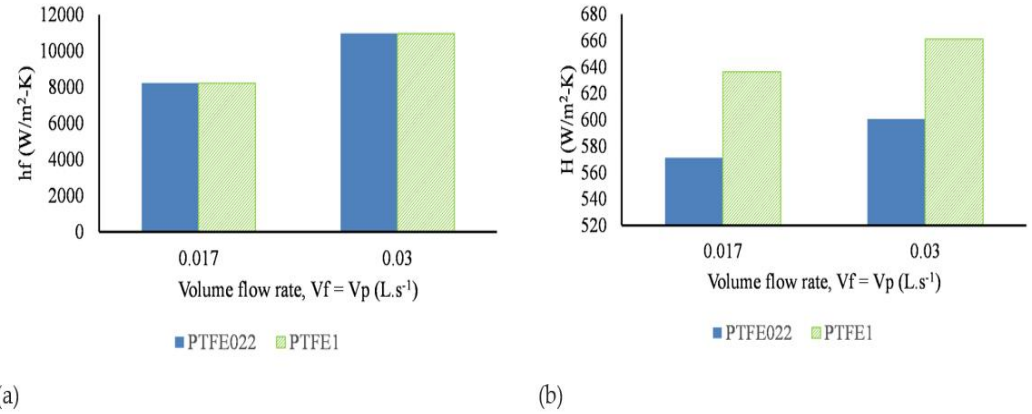

(a) (b)

Figure 9 The impact of volume flow rate on (a) convective heat transfer coefficient, and (b) total heat transfer coefficient in spacer-filled DCMD channels

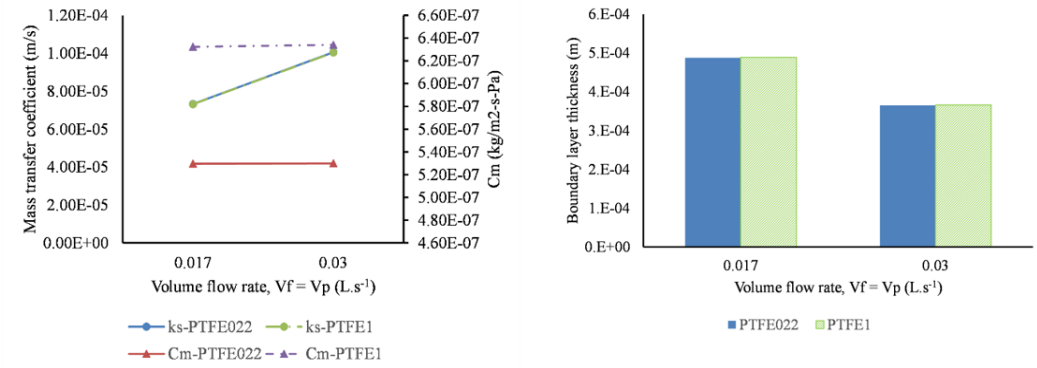

(a) (b)

Figure 10 The impact of volume flow rate on (a) mass transfer coefficient and (b) boundary layer thickness in spacer-filled DCMD channels.

Figure 11 and Figure 12 described that there was an increase in TPC and a decrease in CPC when the volume flow rate went up in both membranes. The boundary layer thickness decreased due to the increase of the volume flow rate, so the temperature difference between the bulk feed side and the feed membrane interface was lower. Consequently, the transmembrane temperature difference was more prominent, and the TPC was higher (Ve et al., 2021a). Furthermore, there were two main factors regarding the reduction of CPC related to the increase in the volume flow rate. Firstly, as mentioned in Eq. (14), the enhancement of permeate production in the investigated range of volume flow rate led to the CPC increase. Secondly, a decrease in the shear stress caused a lower concentration difference between the bulk and membrane surface Ve et al., (2021a); therefore, the concentration polarization effect is reduced. Also, according to Bouchrit et al., (2015), the latter factor was considered dominant for decreasing CPC in this case.

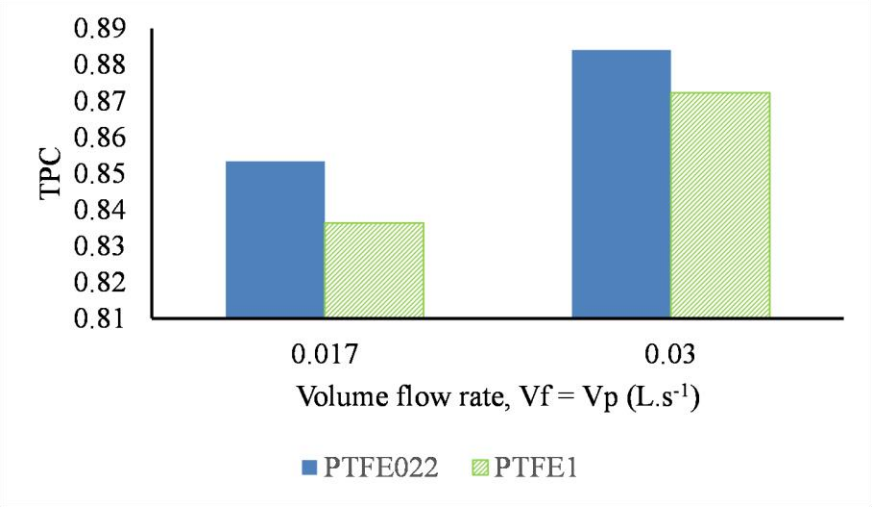

Figure 11 The effect of volume flow rate on the TPC in spacer-filled DCMD configuration

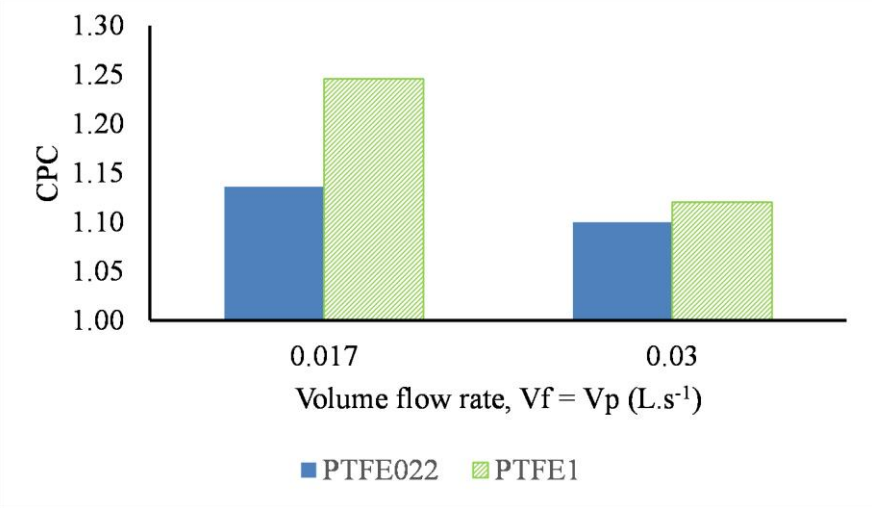

Figure 12 The effect of volume flow rate on the CPC in spacer-filled DCMD configuration

For membranes with larger pore sizes, more water molecules evaporated from the feed side to the permeate side. Thus, the temperature difference between at bulk solution and at membrane surface was more considerable, and the non-volatile matters accumulated more and more on the membrane surface. Consequently, the temperature polarization effect and concentration polarization effect were more severe. Therefore, in comparison to the PTFE022 membrane, the PTFE1 membrane obtained lower TPC values and higher CPC values, as shown in (Figure 11, 12).

Effect of feed concentration on heat and mass transfer rates

This section explored the impact of feed concentration on heat and mass transfer rates. The experimental conditions were Case III of (Table 3). From Figure 13, there was a slight decrease of nearly 1.5% in mass flux for both membranes when the feed concentration rose from 20,000 ppm to 40,000 ppm. As mentioned in previous studies Bouchrit et al., (2015), Alklaibi and Lior, (2006), the feed concentration has no or little influence on mass fluxes if the feed concentration was in the range of (17,750 ppm – 50,000 ppm).

Further, according to Bouchrit et al., (2015), the mass flux dropped considerably by 56% when the feed concentration rose to 177,500 ppm. The water activity was reduced because of the rise of the mole fraction of the feed solution, which caused the drop in the difference of partial vapor pressure between two sides of DCMD channels, as shown in Eq. (19) (Khayet and Matsuura, 2011;

Alkhudhiri et al., 2012; Schofield et al., 1987). However, the fluctuation in water activity was trivial in the investigated feed concentration, which led to a slight change in the partial vapor pressure difference.

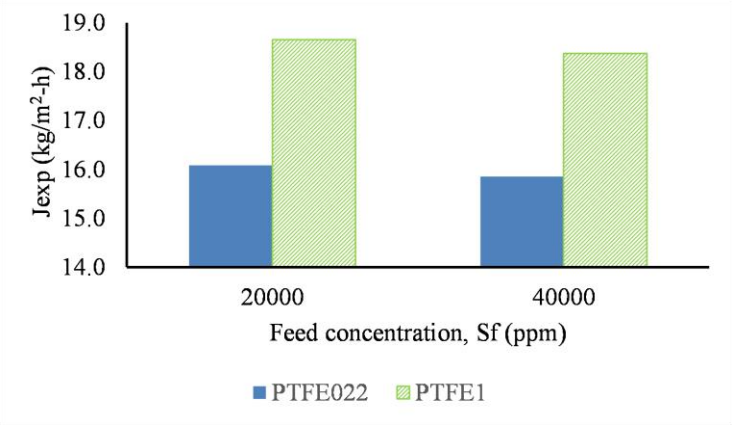

Figure 13 The impact of feed concentration on mass flux

Furthermore, the drop of permeate flux was also reflected through the change of mass transfer coefficient through the boundary layer, permeability coefficient, and boundary layer thickness. Figure 14 showed that the boundary layer thickness increased by nearly 2%, whereas ks and Cm coefficients decreased by under 1% when the feed concentration rose.

$$a_{w,f} = 1 - x_f - 10x_f^2$$
$$p_{v,sf} = a_{w,f} \times p_{v,wf} \quad (19)$$
$$p_{v,wf} = exp\left(23.238 - \frac{3841}{T_{m,f} - 45}\right)$$

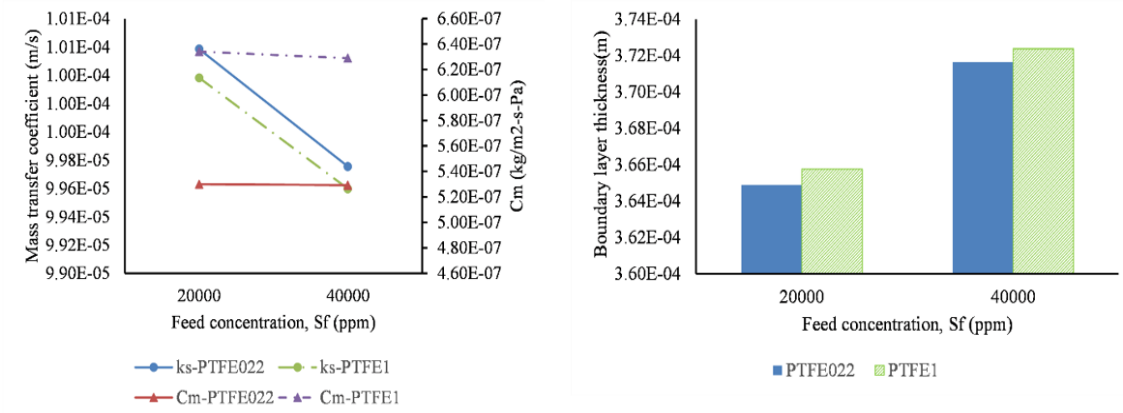

(a) (b)

Figure 14 The impact of feed solution on (a) mass transfer coefficient and (b) boundary layer thickness in spacer-filled DCMD channels.

As shown in Figure 15, the TPC showed a minimal increase in feed concentration. This slight increase in TPC can be attributed to two main factors. Firstly, as illustrated in Figure 16, hf decreased slightly, with nearly 1.3% for both membranes. This decrease is a result of the marginal increase in both the kinematic and dynamic viscosity of saline water. Thus, the Reynolds number reduced slightly when the concentration of feed solution was in the range of 20,000 ppm - 40,000 ppm (Alkhudhiri et al., 2012). Secondly, the expansion of the boundary layer thickness and lower mass fluxes led to a decreased heat flux on the feed side. This resulted in a lower temperature gradient in the boundary liquid layer (T_f-T_(m,f)), which was the dominant factor contributing to the increase of TPC as the feed concentration rose (Martínez-Díez and Vázquez-González, 1999; Suleman et al., 2021; Termpiyakul et al., 2005).

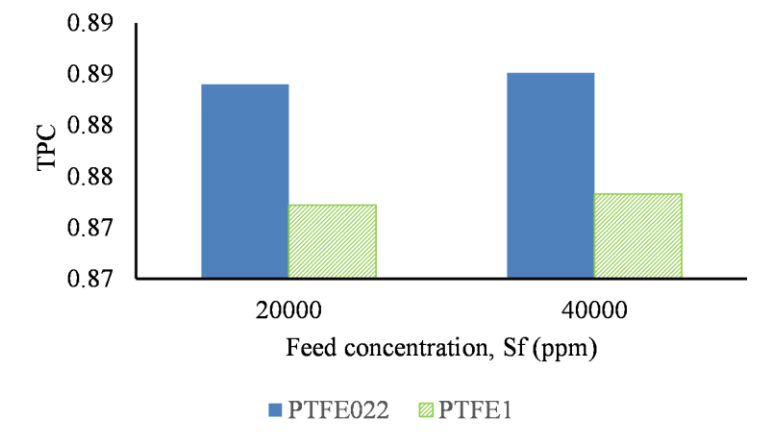

Figure 15 The effect of feed concentration on the TPC

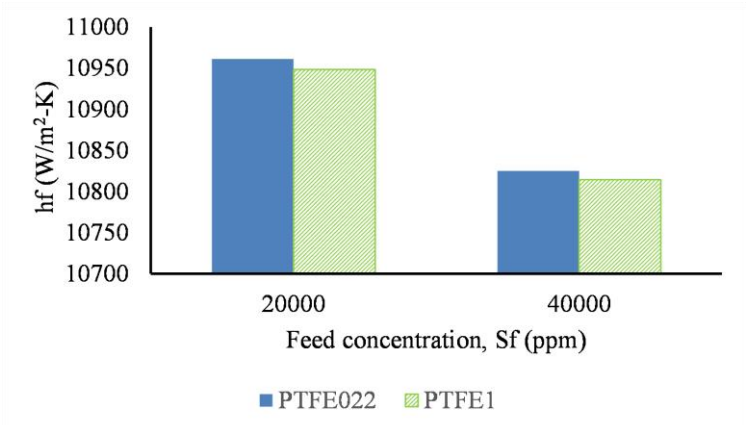

Figure 16 The impact of feed concentration on convective heat transfer coefficient

As indicated in Eq. (13) and Eq. (14), the decline in mass flux resulting from the rise in feed concentration caused a decrease in CPC, meaning that the concentration difference between the bulk solution and the membrane surface was reduced (Bouchrit et al., 2015). However, there was only a 0.2% and 0.4% reduction in CPC for PTFE022 and PTFE1, respectively. Additionally, PTFE1 exhibited a lower TPC (Figure 15) and a higher CPC (Figure 17) compared to PTFE022, attributed to the greater evaporation of water molecules through a larger membrane pore size.

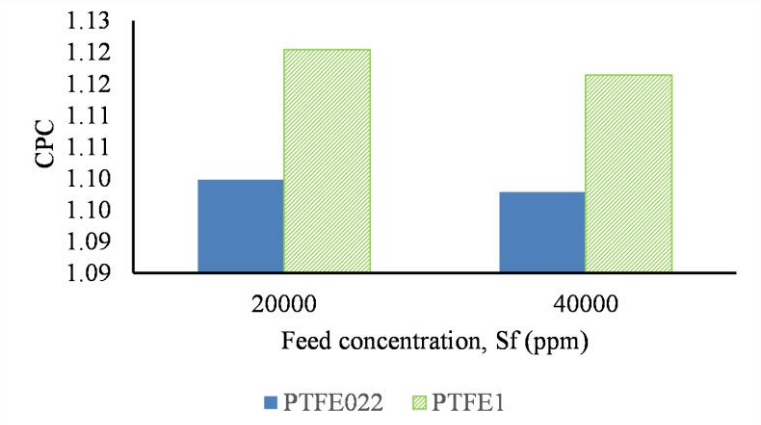

Figure 17 The effect of feed concentration on the CPC in spacer-filled DCMD configuration

4. CONCLUSIONS

The thin film theory and boundary layer theory were used to investigate heat and mass transfer characteristics in spacer-filled DCMD configurations under the impact of different experimental conditions and various pore sizes of hydrophobic PTFE membranes. The relationship between the mass transfer coefficient through the boundary layer, the boundary layer thickness, and DCMD performance was explained in more detail based on this approach. The mass transfer coefficient through the boundary layer, boundary layer thickness, internal heat transfer coefficient, TPC, and CPC underwent substantial changes under the impact of operating conditions.

The feed inlet temperature was the most influential factor on permeate fluxes compared to volume flow rate and feed concentration. At 500C feed inlet temperature, the mass fluxes rose more than 93% for PTFE022 and PTFE1 membranes compared to the recorded values at 400C. The substantial improvement of mass fluxes can be attributed to the significant change in the total heat transfer coefficient. In contrast, the rise of mass fluxes under the effect of volume flow rate can be attributed to the substantial change in the internal heat transfer coefficient instead of the fluctuation of the total heat transfer coefficient. However, the pore size of membranes exerted a pronounced impact solely on the membrane permeability coefficient, TPC, and CPC. Notably, there was negligible effect of the membrane pore size on the mass transfer coefficient of particles, boundary layer thickness, and the internal heat transfer coefficient.

Acknowledgment

We thank the participants who all contributed to the study. We also thank HUE UNIVERSITY who supported the fund for this research.

Author Contributions

Conceptualization, Linh Ve and Farzaneh Mahmoudi; Investigation, Cuong Nguyen and Huy Nguyen; Methodology, Linh Ve, Cuong Do and Lich Nguyen; Software, Linh Ve and Tuan Hoang; Supervision, Linh Ve; Validation, Linh Ve, Cuong Do, Lich Nguyen and Farzaneh Mahmoudi; Visualization, Cuong Nguyen, Huy Nguyen and Tuan Hoang; Writing – original draft, Linh Ve; Writing – review & editing, Farzaneh Mahmoudi. All authors have read and agreed to the published version of the manuscript.

Ethical issues

Not applicable

Informed consent

Not applicable.

Funding

This study was funded by HUE UNIVERSITY, (grant number DHH2022-02-162).

Conflict of Interest

The author declares that there are no conflicts of interests.

Data and materials availability

All data associated with this study are present in the paper.

Nomenclature

A	–	Membrane area, m2
Cm	–	Membrane permeability, kg.m-2.s-1.Pa-1
CPC	–	Concentration polarization coefficient
D		Diffusion coefficient of solute, m2.s-1
Dh	–	Hydraulic diameter for empty channels, m

Jw	–	Experimental mass flux, kg.m-2.s-1
H	–	Overall heat transfer coefficient, W.m-2.K-1
$\Delta H_{v,w}$	–	Vapour enthalpy of water, kJ/kg
L	–	Length of flow channel, m
M	–	Molecular weight of water, kg.mol-1
Nu	–	Nusselt number
Pm	–	Mean pressure within the membrane pores (or total pressure), Pa
Pr	–	Prandtl number
Qf	–	Heat transfer rate through feed thermal boundary layer, W
Qm	–	Heat transfer rate through the membrane, W
Qp	–	Heat transfer rate through permeate thermal boundary layer, W
R	–	Gas constant, J.mol-1.K-1
Re	–	Reynolds number
Sf	–	Feed inlet concentration, ppm
Sm,f	–	Concentration on membrane surface at feed side, ppm
Sc	–	Schmidt number
Sh	–	Sherwood number
Tf	–	Bulk feed side temperature, K
Tm	–	Mean temperature at membrane surface, K
Tm,f	–	Temperature at the feed-membrane interface, K
Tm,p	–	Temperature at the permeate-membrane interface, K
Tp	–	Bulk permeate side temperature, K
TPC	–	Temperature polarization coefficient
Vf	–	Volume flow rate at feed side, L.s-1
Vp	–	Volume flow rate at permeate side, L.s-1
df	–	Filament diameter, m
dh	–	Hydraulic diameter for spacer-filled channels, m
hf	–	Heat transfer coefficient at feed side, W.m-2.K-1
hm	–	Heat transfer coefficient of the whole membrane, W.m-2.K-1
hp	–	Heat transfer coefficient at permeate side, W.m-2.K-1
kdc	–	Correction factor
kg	–	Thermal conductivity of gas phase, W.m-1.K-1
km	–	Thermal conductivity of membrane, W.m-1.K-1
kp	–	Thermal conductivity of membrane material, W.m-1.K-1
ks	–	Mass transfer coefficient through boundary layers, m.s-1
lm	–	Mesh size, m
pa	–	Entrapped air pressure, Pa
pv,sf	–	Partial pressure of water vapour at feed-membrane surface, Pa
pv,sp	–	Partial pressure of water vapour at permeate-membrane surface, Pa
pv,wf	–	Partial vapour pressure of the pure water, Pa
r	–	Mean pore size radius, m
t	–	Thickness of flow channel, m
ts	–	Spacer thickness, m
x	–	Mole fraction of feed solution

Greek symbols		
τ	–	Membrane tortuosity
εm	–	Membrane porosity
ε	–	Spacer porosity
δm	–	Membrane thickness, m
δ	–	Boundary layer thickness, m
θ	–	Angle between filaments of spacer, deg.
ϱ	–	Density of fluid, kg.m-3
αw,f	–	Water activity
Subscripts		
f	–	Feed
p	–	Permeate

REFERENCES

1. Aas GAS, Ali MEA, Shawky HA, Abdel-Mottaleb MSA. Effect of different salts on mass transfer coefficient and inorganic fouling of TFC membranes. J Membr Sci Technol 2017; 7(2):175. doi: 10.4172/2155-9589.1000175
2. Adnan S, Hoang M, Wang H, Xie Z. Commercial PTFE membranes for membrane distillation application: effect of microstructure and support material. Desalination 2012; 284 (4):297-308. doi: 10.1016/j.desal.2011.09.015
3. Alkhudhiri A, Darwish N, Hilal N. Membrane distillation: a comprehensive review. Desalination 2012; 287(15):2-18. doi: 10.1016/j.desal.2011.08.027
4. Alklaibi AM, Lior N. Heat and mass transfer resistance analysis of membrane distillation. J Membr Sci 2006; 282(1-2): 362-369. doi: 10.1016/j.memsci.2006.05.040
5. Andrjesdóttir Ó, Ong CL, Nabavi M, Paredes S, Khalil ASG, Michel B, Poulikakos D. An experimentally optimized model for heat and mass transfer in direct contact membrane distillation. Int J Heat Mass Transf 2013; 66:855-867. doi: 10.1016/j.ijheatmasstransfer.2013.07.051
6. Ashoor BB, Mansour S, Giwa A, Dufour V, Hasan SW. Principles and applications of direct contact membrane distillation (DCMD): a comprehensive review. Desalination 2016; 398:222-246. doi: 10.1016/j.desal.2016.07.043
7. Bahmanyar A, Asghari M, Khoobi N. Numerical simulation and theoretical study on simultaneously effects of operating parameters in direct contact membrane distillation. Chem Eng Process 2012; 61:42-50. doi: 10.1016/j.cep.2012.06.012
8. Banat FA, Simandl J. Desalination by membrane distillation: a parametric study. Sep Sci Technol 1998; 33(2):201-226. doi: 10.1080/01496399808544764
9. Bouchrit R, Boubakri A, Hafiane A, Bouguecha SAT. Direct contact membrane distillation: capability to treat hyper-saline solution. Desalination 2015; 376:117-129. doi: 10.1016/j.desal.2015.08.014
10. Boudinar MB, Hanbury WT, Avlonitis S. Numerical simulation and optimisation of spiral-wound modules. Desalination 1992; 86(3):273-290. doi: 10.1016/0011-9164(92)80038-B
11. Camacho ML, Dumée L, Zhang J, Li Jd, Duke M, Gomez J, Gray S. Advances in membrane distillation for water desalination and purification applications. Water 2013; 5(1):94-196. doi: 10.3390/w5010094
12. Chang H, Hsu JA, Chang CL, Ho CD, Cheng TW. Simulation study of transfer characteristics for spacer-filled membrane distillation desalination modules. Appl Energy 2017; 185(P2): 2045-2057. doi: 10.1016/j.apenergy.2015.12.030
13. Chen TC, Ho CD, Yeh HM. Theoretical modeling and experimental analysis of direct contact membrane distillation. J Membr Sci 2009; 330(1-2):279-287. doi: 10.1016/j.memsci.2008.12.063
14. Curcio E, Drioli E. Membrane distillation and related operations: a review. Sep Purif Rev 2005; 34(1):35-86. doi: 10.1081/SPM-200054951
15. Ding Z, Ma R, Fane AG. A new model for mass transfer in direct contact membrane distillation. Desalination 2003; 151 (3):217-227. doi: 10.1016/S0011-9164(02)01014-7
16. Dittscher U, Woermann D, Wiedner G. Temperature polarization in membrane distillation of water using a porous hydrophobic membrane. Bur Bunsen Phys Chem 1994; 98(8):1056-1061. doi: 10.1002/bbpc.19940980810
17. Drioli E, Ali A, Macedonio F. Membrane distillation: recent developments and perspectives. Desalination 2015; 356:56-84. doi: 10.1016/j.desal.2014.10.028

18. El-Bourawi MS, Ding Z, Ma R, Khayet M. A framework for better understanding membrane distillation separation process. J Membr Sci 2006; 285(1):4-29. doi: 10.1016/j.mems ci. 2006.08.002
19. García-Payo MC, Izquierdo-Gil MA. Thermal resistance technique for measuring the thermal conductivity of thin microporous membranes. J Phys D: Appl Phys 2004; 37:3008-3 016. doi: 10.1088/0022-3727/37/21/011
20. Katsandri A. A theoretical analysis of a spacer filled flat plate membrane distillation modules using CFD-Part I: velocity and shear stress analysis. Desalination 2017a; 408:145-165. doi: 10.1 016/j.desal.2015.09.001
21. Katsandri A. A theoretical analysis of a spacer filled flat plate membrane distillation modules using CFD-Part II: temperature polarisation analysis. Desalination 2017b; 408:16 6-180. doi: 10.1016/j.desal.2015.11.021
22. Khalifa A, Ahmad H, Antar M, Laoui T, Khayet M. Experimental and theoretical investigations on water desalination using direct contact membrane distillation. Desalination 2017; 404:22-34. doi: 10.1016/j.desal.2016.10.009
23. Khayet M. Membranes and theoretical modeling of membrane distillation: a review. Adv Colloid Interface Sci 2011; 164(1):56 -88. doi: 10.1016/j.cis.2010.09.005
24. Khayet M. Solar desalination by membrane distillation: dispersion in energy consumption analysis and water production costs (a review). Desalination 2013; 308:89-101. doi: 10.1016/j.desal.2012.07.010
25. Khayet M, Matsuura T. Membrane distillation: principles and applications. Elsevier 2011. doi: 10.1016/B978-0-444-53126-1.10 001-6
26. Khayet M, Godino MP, Mengual JI. Modelling transport mechanism through a porous partition. J Non-Equil Thermodyn 2001; 26(1):1-14. doi: 10.1515/JNETDY.2001.001
27. Lawson KW, Lloyd DR. Membrane distillation. J Membr Sci 1997; 124(1):1-25. doi: 10.1016/S0376-7388(96)00236-0
28. Li F, Meindersma W, De-Haan AB, Reith T. Optimization of commercial net spacers in spiral wound membrane modules. J Membr Sci 2002; 208(1):289-302. doi: 10.1016/S0376-7388(02)00 307-1
29. Lokare OR, Vidic RD. Impact of operating conditions on measured and predicted concentration polarization in membrane distillation. Environ Sci Technol 2019; 53(20):11869 -11876. doi: 10.1021/acs.est.9b04182
30. Martínez L, Florido-Díaz FJ. Theoretical and experimental studies on desalination using membrane distillation. Desalination 2001; 139(1):373-379. doi: 10.1016/S0011-9164(01) 00335-6
31. Martínez-Díez L, Vázquez-González MI. Temperature and concentration polarization in membrane distillation of aqueous salt solutions. J Membr Sci 1999; 156(2):265-273. doi: 10.1016/S0376-7388(98)00349-4
32. Martínez-Díez L, Florido-Díaz FJ, Vázquez-González MI. Study of polarization phenomena in membrane distillation of aqueous salt solutions. Sep Sci Technol 2000; 35(10):1485-1501. doi: 10.1081/SS-100100237
33. Nayar KG, Sharqawy MH, Banchik LD, Lienhard VJH. Thermophysical properties of seawater: a review and new correlations that include pressure dependence. Desalination 2016; 390:1-24. doi: 10.1016/j.desal.2016.02.024
34. Olatunji SO, Camacho LM. Heat and mass transport in modeling membrane distillation configurations: a review. Front Energy Res 2018; 6:130. doi: 10.3389/fenrg.2018.00130
35. Phattaranawik J, Jiraratananon R, Fane AG. Heat transport and membrane distillation coefficients in direct contact membrane distillation. J Membr Sci 2003; 212(1-2):177-193. doi: 10.1016/S0376-7388(02)00498-2
36. Plamenov HI. Model-based analysis and optimization of membrane distillation. Ghent University, Faculty of Bioscience Engineering, Ghent, Belgium, 2017.
37. Qtaishat M, Matsuura T, Kruczek B, Khayet M. Heat and mass transfer analysis in direct contact membrane distillation. Desalination 2008; 219(1-3):272-292. doi: 10.1016/j.desal.2007.0 5.019
38. Rodríguez-Maroto JM, Martínez L. Bulk and measured temperatures in direct contact membrane distillation. J Membr Sci 2005; 250(1-2):141-149. doi: 10.1016/j.memsci.2004.09.046
39. Saeed A, Vuthaluru R, Vuthaluru HB. Investigations into the effects of mass transport and flow dynamics of spacer filled membrane modules using CFD. Chem Eng Res Des 2015; 93:7 9-99. doi: 10.1016/j.cherd.2014.07.002
40. Schlichting H, Kestin J. Boundary layer theory (7th ed.). McGraw-Hill Book Company, New York, 1979. doi: 10.1115/1 .3240614
41. Schock G, Miquel A. Mass transfer and pressure loss in spiral wound modules. Desalination 1987; 64:339-352. doi: 10.1016/0 011-9164(87)90107-X
42. Schofield RW, Fane AG, Fell CJD. Gas and vapour transport through microporous membranes. I. Knudsen-Poiseuille transition. J Membr Sci 1990; 53(1-2):159-171. doi: 10.1016/037 6-7388(90)80011-A
43. Schofield RW, Fane AG, Fell CJD. Heat and mass transfer in membrane distillation. J Membr Sci 1987; 33(3):299-313. doi: 1 0.1016/S0376-7388(00)80287-2

44. Shakaib M, Hasani SMF, Mahmood M. CFD modeling for flow and mass transfer in spacer-obstructed membrane feed channels. J Membr Sci 2009; 326(2):270-284. doi: 10.1016/j.memsci.2008.09.052
45. Singh D, Sirkar KK. High temperature direct contact membrane distillation based desalination using PTFE hollow fibers. Chem Eng Sci 2014; 116:824-833. doi: 10.1016/j.ces.2014.05.042
46. Sudoh M, Takuwa K, Iizuka H, Nagamatsuya K. Effects of thermal and concentration boundary layers on vapor permeation in membrane distillation of aqueous lithium bromide solution. J Membr Sci 1997; 131(1-2):1-7. doi: 10.1016/S0376-7388(97)00109-9
47. Suleman M, Asif MB, Jamal SA. Temperature and concentration polarization in membrane distillation: a technical review. Desalination Water Treat 2021; 229:52-68. doi: 10.5004/dwt.2021.27398
48. Taamneh Y, Bataineh K. Improving the performance of direct contact membrane distillation utilizing spacer-filled channel. Desalination 2017; 408:25-35. doi: 10.1016/j.desal.2017.01.004
49. Termpiyakul P, Jiraratananon R, Srisurichan S. Heat and mass transfer characteristics of a direct contact membrane distillation process for desalination. Desalination 2005; 177(1-3):133-141. doi: 10.1016/j.desal.2004.11.019
50. Tewodros BN, Yang DR, Park K. Design parameters of a Direct Contact Membrane Distillation and a case study of Its applicability to low-grade waste energy. Membranes (Basel) 2022; 12(12):1279. doi: 10.3390/membranes12121279
51. Ve QL, Koirala R, Bawahab M, Faqeha H, Do MC, Nguyen QL, Date A, Akbarzadeh A. Experimental investigation of the effect of the spacer and operating conditions on mass transfer in direct contact membrane distillation. Desalination 2021a; 500:114839. doi: 10.1016/j.desal.2020.114839
52. Ve QL, Koirala R, Bawahab M, Faqeha H, Do MC, Nguyen QL, Date AS, Akbarzadeh A. Theoretical modelling and experimental study of spacer-filled direct contact membrane distillation: Effect of membrane thermal conductivity model selection. Desalination Water Treat 2021b; 217:63-73. doi: 10.5004/dwt.2021.26921
53. Ve QL, Rahaoui K, Bawahab M., Faqeha H, Date A, Faghih A, Akbarzadeh A. An experimental heat transfer investigation of using spacer in direct contact membrane distillation. Energy Procedia 2019; 160:223-230. doi: 10.1016/j.egypro.2019.02.140
54. Yun Y, Ma R, Zhang W, Fane AG, Li J. Direct contact membrane distillation mechanism for high concentration NaCl solutions. Desalination 2006; 188(1-3):251-262. doi: 10.1016/j.desal.2005.04.123
55. Yun Y, Wang J, Ma R, Fane AG. Effects of channel spacers on direct contact membrane distillation. Desalination Water Treat 2011; 34(1-3):63-69. doi: 10.5004/dwt.2011.2870